Raman scattering interferences as a probe of vertical coherence in multilayers of carbon-induced Ge quantum dots

P. D. Lacharmoise,* A. Bernardi, A. R. Goñi, M. I. Alonso, and M. Garriga
Institut de Ciència de Materials de Barcelona-CSIC, Esfera UAB, 08193 Bellaterra, Spain

N. D. Lanzillotti-Kimura and A. Fainstein
Centro Atómico Bariloche-Instituto Balseiro, CNEA, San Carlos de Bariloche, 8400 Río Negro, Argentina
(Received 25 June 2007; revised manuscript received 2 August 2007; published 16 October 2007)

We have probed the effect of disorder in the vertical alignment of Ge quantum dots of a multilayered structure by means of Raman scattering. Despite of using a thin Si spacer of 20 nm between dot layers, the coherent piling up of Ge dots one on top of the other is fully suppressed by the deposition of a submonolayer of carbon prior to the dot growth in each layer. For stacks with perfect dot correlation in the growth direction, the interaction of acoustic phonons with the ensemble of electronic states confined to the dots gives rise to well defined Raman interferences. The interference contrast almost vanishes when carbon is introduced on the dot-nucleation surfaces. Instead, a strong and decreasing background is observed at small Raman shifts. These drastic changes in the Raman spectra of dot multilayers with and without C are very well reproduced by simulations based on the interference model of Cazayous *et al.* [Phys. Rev. B **62**, 7243 (2000)].

DOI: 10.1103/PhysRevB.76.155311 PACS number(s): 78.30.−j, 78.67.Pt, 63.20.Kr, 81.07.Ta

I. INTRODUCTION

Self-assembled Ge quantum dots (QDs) attracted a lot of attention in recent years because of their great potential as building blocks in semiconductor nanodevices, which are compatible with Si-based technology. In particular, Ge-dot multiple-layer structures have been widely studied for their promising engineering possibilities, for example, in thermoelectric applications and even optoelectronics.[1–4] To achieve materials with improved thermoelectric properties, a precise control of the morphology and the spatial distribution of the quantum dots is required. For the Si/Ge material system, a possible pathway consists in the deposition of a small amount of carbon, which is known to induce drastic changes in the dot formation mechanism.[5–8] In this way, one has a handle not only on the dot morphology but also on its density and, what is of crucial importance for our work, on the vertical correlation of the dots among different layers. The latter is because self-assembled dot multilayers exhibit long-range ordering across the multiple layers. For a review on the possible arrangements of QDs in stacks, we refer to the work of Stangl *et al.* and references therein.[9] Such a coherent dot growth is driven by the strain field surrounding a dot that propagates, hence producing a vertical alignment of the dots from one layer to the next.[10,11] Only sufficiently large Si spacers between dot layers are able to erase this strain memory, suppressing any interlayer correlation. Here, we are particularly interested in the possibility of designing quantum-dot multiple-layer structures with uncorrelated dots independent of the Si spacer thickness by adding C to the system. Since C is roughly speaking about 50% smaller than Si, the deposition of a submonolayer of C on the nucleation surface for the Ge-dot growth induces locally strong strain fields upon C incorporation. These inhomogeneities drastically reduce the mobility of the oncoming Ge atoms, which neutralizes any seeding effect for QD nucleation due to the presence of a dot in the underlying layer.[6]

In order to address the vertical coherence in C-induced Ge-dot multilayers, we performed Raman scattering experiments in the acoustic-phonon region. The photoelastic model has been typically used to describe the inelastic light scattering by acoustic phonons in superlattices.[12,13] A correct description of both the photoelastic and the acoustic modulation is necessary in order to properly outline the features in Raman spectra of multilayered systems.[14] Variations of this model were developed for the case of resonant and out-of-resonance Raman scattering. Whereas an assignment of a photoelastic constant to each material of the superlattice is enough to describe systems out of resonance, the electron-phonon interaction and thus the distribution of electronic states must be taken into account explicitly in the resonant case. Ruf *et al.* addressed this problem when studying the effects of thickness fluctuations in quantum wells, giving a microscopic description of the photoelastic Raman-scattering mechanism by considering the interaction between acoustic phonons and confined electronic states explicitly.[15–17] The importance of finite sample effects and a precise calculation of the phonon modes in superlattices and quasiperiodical systems were discussed in subsequent works.[18–21] The concept of Raman interferences by acoustic-phonon scattering, however, was introduced by Giehler *et al.*[22] Finally, Cazayous *et al.* clearly demonstrated how acoustic phonons can interact with the ensemble of electronic confined states in multiple layers of dots, thus giving rise to pronounced Raman scattering interferences.[23–27] Within this model, the Raman intensity results from a real interference of the inelastically scattered photons by acoustic phonons in processes mediated by electrons confined to different quantum dots. Hence, the spatial arrangement of the quantum dots might play a crucial role. In fact, as discussed in previous works,[23–27] we show here both experimentally and theoretically that making use of the sensitivity of Raman scattering to the spatial ordering of quantum dots in multilayered systems, we are able to unravel the strong randomization in-

duced by C deposition on QD nucleation, which cares less about the strain field extending from layer to layer.

II. EXPERIMENTAL DETAILS AND SPECTRA

We designed two multiple-layer structures grown by solid-source molecular beam epitaxy on the same Si(001) wafer under identical conditions, except for the way C was used to influence the dot nucleation in each heterostructure. A different C-deposition sequence was readily achieved by shuttering half of the wafer area in certain C evaporation steps. First, a 100 nm thick Si buffer layer was deposited. Then, the temperature was set to 500 °C to proceed with the layer structure. It consists of an eightfold stack of self-assembled Ge dots separated by a 20 nm thick Si spacer. This thickness ensures that in the absence of C, the Ge dots are vertically correlated. The first period was identical in the two samples: a 4 Å thick Ge wetting layer was grown before depositing 0.1 monolayer of carbon to control the shape and density of the quantum dots.[7,8] In the next step, 7 Å of Ge was deposited for the dots to nucleate, which was capped with the 20 nm thick Si spacer, completing the period. Adopting this procedure, a typical dot shape of ~6 nm height and ~40 nm base size with a density of about 40 dots/μm^2 is obtained.[7,8] The remaining seven periods were grown using the shutter to cover half wafer during C deposition. In this way, we obtain two samples with similar dot parameters such as size and density but in the region where no C is present, an almost perfect vertical correlation is expected, whereas in the area with C deposited in each period, such correlation should be totally destroyed.[6] Hereafter, we will refer to the multilayers as "without C" and "with C," respectively. The vertical arrangement of the Ge dots in each case was further confirmed by transmission electron microscopy.

Raman spectra were collected at room temperature with a Jobin-Yvon T64000 triple spectrometer in subtractive mode. The spectral resolution was about 2 cm^{-1}. The scattering configuration was close to the backscattering geometry. We used the lines of an Ar-Kr laser ranging from 2.18 eV (red) to 2.54 eV (blue) for excitation. Figure 1 shows measured Raman spectra of both multilayers with and without C for different laser lines with photon energies around that of the E_1 interband transition of the Ge quantum dots. Due to the large energy width of the resonance curve for this transition,[28] resonance conditions are easily fulfilled for the whole dot ensemble. The spectra of the two samples are qualitatively different, revealing the drastic effect of C deposition on the vertical alignment of the dots. The Raman spectrum of the multilayer without C displays a clear interference pattern, whereas the one with C shows a decaying signal slightly modulated when exciting at 2.54 eV. For the multilayer without C, the maximum interference contrast is attained for blue excitation at 2.5 eV, slowly decreasing as one moves away from the resonance to completely disappear at around 1.91 eV. A similar resonant behavior is observed for the intensity of the decaying signal in the spectra of the multilayer with C.

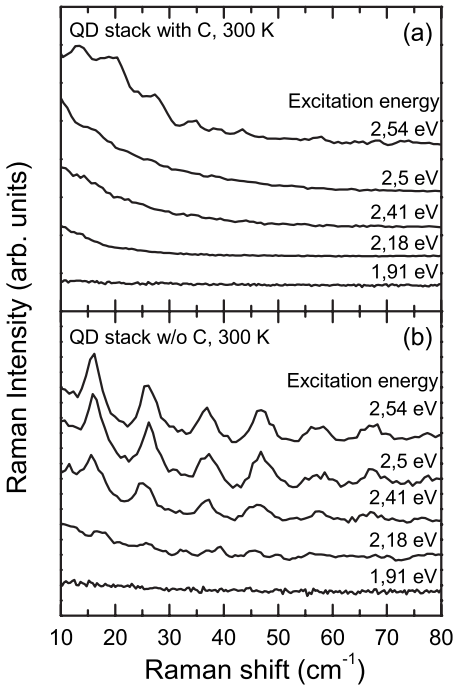

FIG. 1. Raman spectra in the acoustic-phonon region of Ge quantum-dot multilayers (a) with and (b) without carbon deposition prior to the dot nucleation measured at room temperature with different laser excitation energies.

III. ANALYSIS

A. Raman interference model

We simulated Raman spectra of our QD stack samples using the three-dimensional model proposed by Cazayous *et al.*[23–25] The analysis of the Raman spectra in many studies of periodic heterostructures was performed on the basis of the photoelastic model and the folding of the phonon dispersion curve due to the superimposed periodicity of the structure.[29–31] However, the validity of this model for finite, low-dimensional systems such as quantum-dot multilayers is arguable. First of all, the Brillouin minizone formation would strictly require an infinite periodical modulation of the acoustical impedance, which is not the case in many studied multiple-layer structures with low number of periods. The finite size of the dots, for instance, is also neglected in such calculations. Moreover, a strictly two-dimensional photoelastic model is completely unable to describe the spatial coherence of the dots from layer to layer. Thus, this kind of simulations would never meet the requirements to distinguish between vertically aligned and randomly distributed dots, as shown below to be the case in Raman scattering experiments.

In the model of Raman interferences, the energy of the measured peaks is only related to the fact of having a constructive interference between photons scattered by acoustic phonons, which interact with the three-dimensional ensemble of electronic states confined to the dots. The interference model takes explicitly into account the effect of electronic confinement since its spectral envelope in the Raman spectrum, i.e., the intensity modulation of the interference peaks,

is determined by the Fourier transform of the electronic wave function and its spatial extension. In our simulations, the quantum dots are treated as identical quantum disks with $\varphi_{n,l_p}(z)$ and $\Psi_{m,l_p}(\vec{r})$ denoting the electronic wave function in the growth direction and the in-plane component, respectively, for confined states with subindices (n,m). The symbols l_p and p denote the layer index and the dot index within that layer, respectively. The lack of translation invariance breaks the wave-vector conservation rules and, therefore, all acoustic phonons may scatter in the Raman process. Considering the deformation potential as the main electron-phonon interaction mechanism between an acoustic phonon with wave vector q and displacement field u_q and the ensemble of electronic states, the Raman intensity is proportional to[16,17,24]

$$I_R \propto \left| \sum_{p,l_p} \vec{q} \cdot \vec{u}_q \int \Psi^*_{m,l_p}(\vec{r}) e^{i(\Delta\vec{k}_\parallel - \vec{q}_\parallel)\cdot\vec{r}} \Psi_{\check{m},l_p}(\vec{r}) d^2r \times \int \varphi^*_{n,l_p}(z) e^{i(\Delta k_z - q_z)\cdot z} \varphi_{\check{n},l_p}(z) dz \right|^2, \quad (1)$$

where Δk_z ($\Delta k_\parallel$) is the difference between the incident and scattered photon wave vector in the growth (in-plane) direction. Identical dots hold that $\varphi_{n,l_p}(z) = \varphi(z - z_p)$ and $\Psi_{m,l_p}(\vec{r}) = \psi(\vec{r} - \vec{r_p})$ where z_p and $\vec{r_p}$ are the spatial coordinates of the dot with index p. Hence, Eq. (1) can be simplified to

$$I_R \propto \overbrace{\left| \int \Psi^*(\vec{r})\Psi(\vec{r}) e^{-i\vec{q}_\parallel\cdot\vec{r}} d^2r \int \varphi^*(z)\varphi(z) e^{-iq_z z} dz \right|^2}^{F} \times \underbrace{\left| \sum_{p,l_p} u_{q,l_p} e^{-i(q_z - \Delta k_z) z_{l_p}} e^{-i(\vec{q}_\parallel - \Delta\vec{k}_\parallel)\cdot\vec{r}_{l_p,p}} \right|^2}_{S} \quad (2)$$

where F and S are the form and structure factor, respectively. F depends only on the electronic confinement within the dots and determines the spectral envelope, whereas S represents the interference pattern coming from the interaction of the extended phonon with the dot ensemble. Periodical oscillations of the Raman signal coming from S are expected if the dot layers are regularly spaced, being the oscillation period inversely proportional to the spacer thickness. A random number generator algorithm is used to determine the in-plane positions of the quantum dots in the first layer of the structure. The obtained in-plane dot distribution is repeated for the subsequent layers in the case of ordered multilayers. On the contrary, a random in-plane distribution for each layer is considered in the case of disordered structures. In order to have sufficient statistics in the calculation, each Raman spectrum is simulated by summing over 200 different configurations.

B. Results and discussion

Figure 2 shows two series of simulated spectra in the case of a sample with vertically correlated dots. All the QD multilayers consist in a stack of eight periods. An effective refractive index of 4.4 and a laser energy of 2.54 eV were used in the calculations. In the first series, the dot parameters are fixed and only the spacer thickness varies. From the form factor in Eq. (2), we infer that the degree of confinement in a specific direction determines the weight of the contribution from phonons traveling in that direction. Since the dot height is about seven times smaller than the base diameter, we are mainly dealing with plane waves with in-plane wave vectors close to zero. In the calculations, we consider for the sake of simplicity that the phonon displacements $u_q(z)$ are solely a function of z. Hence, to a good approximation, the physical picture is that of two counterpropagating plane waves with crystal momentum $\pm q_z$ and sound velocity V_{eff} traveling simultaneously. The condition to obtain a maximum in the interference pattern is $q_z \pm \Delta k_z = 2\pi n/L$, where L and n are the spacer thickness and an integer, respectively. Doublets of order n with a fixed energy separation of $2\Delta k_z V_{eff}$ are expected. In the upper part of Fig. 2, the dotted lines indicate the shift of the doublets of orders 1 and 2. The separation between different doublets diminishes as the spacer thickness increases. Since the shift of the peaks is proportional to n, contributions from doublets with different n can merge to form new doublets, as is the case of the spectrum for $L = 20$ nm.

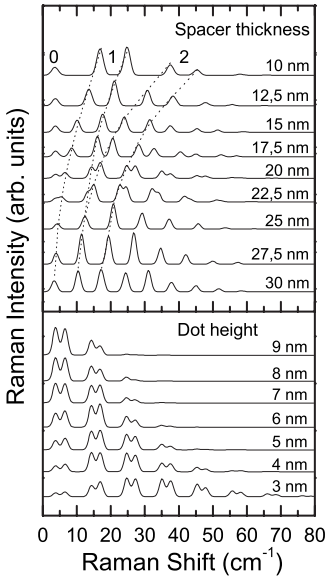

FIG. 2. Series of simulated Raman spectra of an ordered Ge-dot multilayer as a function of the spacer thickness (top panel) and the dot dimensions (bottom panel). The former dots of 4 nm height and 27 nm base size were considered. In the latter case, a fixed spacer thickness equal to 20 nm and an aspect ratio of 0.15 were used.

In the lower panel of Fig. 2, we display the simulated Raman spectra of multilayers with a Si spacer of 20 nm but where the height and the base diameter of the dots were varied at a fixed aspect ratio. We note that the width of the spectral envelope which modulates the intensity of the interference peaks increases with decreasing dot size, i.e., for stronger confinement of the electronic states. The model is not only clearly sensitive to the spatial distribution of the

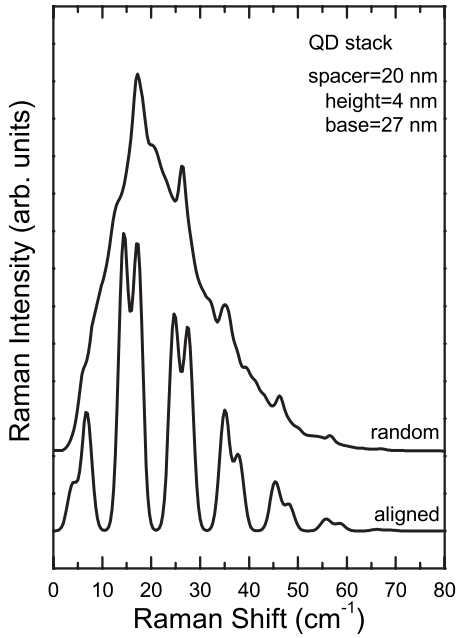

FIG. 3. Simulated Raman spectra of two Ge-dot multilayer structures both with the same parameters but differing only in the spatial correlation of the dots in the growth direction. The lower and upper curves were calculated with vertically correlated (aligned) and uncorrelated (random) dots, respectively.

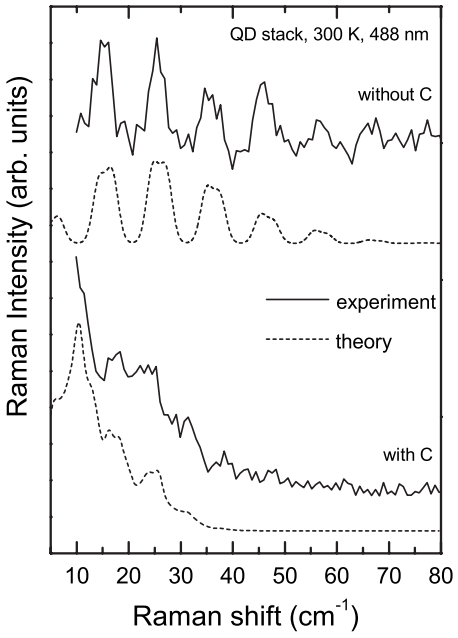

FIG. 4. (Solid curves) Measured Raman spectra of Ge-dot multiple-layer samples with and without carbon. The dashed curves represent the corresponding spectra simulated using the Raman interference model (see text for details).

dots but also to the extent of the electronic wave functions.

Figure 3 displays two spectra calculated for the same multilayer consisting in QD stacks of eight periods, which differ only in the vertical ordering of the dots, as described before. The upper one has randomly distributed dots within the first dot layer but exactly the same dot pattern is repeated in the subsequent layers, leading so to perfect stacking in the growth direction. The spectrum exhibits high-contrast interferences. The lower spectrum corresponds to the case of randomly distributed dots in every layer without interlayer correlation. The interferences blur almost completely, giving a continuum contribution modulated by the form factor envelope. Nevertheless, faint interference peaks on top of the envelope remain visible even for the disordered dot distribution. These effects are thus expected to show up in resonant Raman spectra in the acoustic-phonon region, allowing us to study the spatial correlation of dots in multilayered systems.

For comparison, both measured and calculated Raman spectra of the samples with and without C are plotted together in Fig. 4. In order to avoid the background signal coming from Rayleigh scattering, a reference spectrum measured on a Si wafer has been subtracted from the experimental spectra. The stray light coming from the laser made impossible to work below 8 cm^{-1} in backscattering geometry because of the surface roughness of the samples. For the simulations, we considered a density of 40 dots/μm^2 and we summed over many dot distributions to prevent finite-size effects of the ensemble. We also performed a convolution using a Gaussian with a width of 2 cm^{-1} in order to account for the experimental line broadening. The calculations are in very good agreement with the experiment, as far as the peak positions and relative intensities are concerned. However, the most compelling evidence that C deposition effectively suppresses the vertical coherence of the dot growth is the striking similarity of the measured and simulated Raman spectra of the stack with C.

The spectrum of the multilayer without C displays clear periodic oscillations coming from the constructive interferences between dot layers. The oscillation period is well accounted for by the simulation, when performed with a spacer thickness of 20 nm. This is in excellent agreement with the nominal growth parameters. The interference contrast is a clear indicator of the spatial correlation between dots in the z direction. In randomly distributed dot stacks, the interferences vanish. This is again well demonstrated by the spectrum of the C-induced Ge dot multilayer, where the deposition of C in each layer has erased the strain memory responsible for a coherent growth of the dots from layer to layer. The simulation with a random distribution across the stack also reproduces the spectral features in this case. We note a slight modulation interference coming from the structure factor contribution on top of an exponential decaying signal. A closer inspection to the structure factor of Eq. (2) reveals that the interferences appear when the contribution from the dots add up coherently. This is determined by the phase which is given by

$$(q_z - \Delta k_z) z_{l_p} + (\vec{q}_{\parallel} - \vec{\Delta k}_{\parallel}) \cdot \vec{r}_{l_p,p}. \tag{3}$$

Both terms in Eq. (3) are independent. The former leads always to interferences since the QD stacks exhibit good periodicity in the z direction regardless of the existence or loss of interlayer correlations due to the introduction of C. The interference blurring comes from the second term

$\vec{q}_{\parallel} \cdot \vec{r}_{l_p,p}$, which introduces a dephasing if the dots are not aligned in the growth direction. The $\vec{q}_{\parallel}$ that participate in the scattering process are defined by the lateral extension of the dot. Since the diameter of the dot is about 60 times the lattice constant of the material, the $\vec{q}_{\parallel}$ that contribute the most are close to zero. Thus, the values of the dephasing term are large enough to blur the interferences but not completely, as observed also in the experimental spectra.

It is important to notice that although a 20 nm thick spacer has been chosen for our samples, the disordering effect of C should be effective for even thinner spacers. Vertically uncorrelated Ge-dot stacks with such thinner spacers would be impossible to achieve with conventional self-assembled dot growth. Unfortunately, it was not possible to study intermediate cases between aligned and randomly distributed dots in the z direction because of the drastic effect that very small amounts of C have on the dot-nucleation mechanism.

We now turn to the discussion of the spectral envelope. As we mentioned before, this envelope depends on the form factor F, which is determined by the electronic density associated with the confined dot states, i.e., it depends on dot dimensions. The envelope for the multilayer without C is well reproduced by the simulations considering dots with 4 nm height and 27 nm base size. In contrast, slightly bigger dots with a height of 6 nm and a base length of 40 nm account better for the envelope in the case of the C-induced quantum dots. This is actually closely related to the QD-growth mechanism itself, which is different in both cases. When carbon is deposited, the nucleation of the Ge dots proceeds immediately, leading to an effective reduction of the critical thickness for the Stranski-Krastanow growth mode.[5–8] If no C is deposited, part of the Ge coverage is used to achieve that critical thickness; hence, the resulting dots are smaller in size compared to those grown using C deposition. As illustrated by the calculated Raman spectra of Fig. 2 (lower panel), the position of the envelope maximum shifts to larger Raman shifts for smaller dot sizes. Such shift is extremely sensitive to changes as small as 1 nm in the height of the dots, which is the dimension leading to the strongest confinement.

IV. CONCLUSIONS

In summary, the multiple-peak structure observed in the spectra of Raman scattering by acoustic phonons of Ge QD stacks with ordered dots along the growth direction is well explained within the model of Raman interferences. From the position of the interference maxima and the relative intensities, it is possible to extract by simulation of the Raman spectra important structural parameters of the dot stacks such as the spacer-layer thickness and average dot height. It was also confirmed that such Raman interferences blur almost completely by total loss of coherence between dots of subsequent layers. In our work, a strong piling disorder was introduced by means of C deposition prior to the QD growth in each layer. The resulting spectra exhibit a smooth envelope in the form of a broad band, with maximum position and width related to the mean dot size. In this way, acoustic-phonon Raman scattering provides us with a powerful analytical, fast, and noninvasive tool for the characterization of the structural properties of QD multilayers for specific applications in SiGe-based thermoelectrical nanodevices.

ACKNOWLEDGMENTS

P.D.L. thanks Groenen and Huntzinger for very fruitful discussions. P.D.L. acknowledges an I3P-CSIC grant and A.B. acknowledges support from FPI program. A.R.G. is supported by ICREA. This work was supported in part by the Spanish Ministerio de Educación y Ciencia through Grant No. MAT2006-02680.

*placharmoise@icmab.es

[1] J. L. Liu, A. Khitun, K. L. Wang, W. L. Liu, G. Chen, Q. H. Xie, and S. G. Thomas, Phys. Rev. B **67**, 165333 (2003).
[2] Y. Bao, W. L. Liu, M. Shamsa, K. Alim, A. A. Balandin, and J. L. Liu, J. Electrochem. Soc. **152**, G432 (2005).
[3] A. A. Shklyaev and M. Ichikawa, Appl. Phys. Lett. **80**, 1432 (2002).
[4] O. G. Schmidt, K. Eberl, and J. Auerswald, J. Lumin. **80**, 491 (1998).
[5] Y. Wakayama, L. V. Sokolov, N. Zakharov, R. Werner, and U. Gösele, Appl. Surf. Sci. **216**, 419 (2003).
[6] O. G. Schmidt, S. Schieker, K. Eberl, O. Kienzle, and F. Ernst, Appl. Phys. Lett. **73**, 659 (1998).
[7] A. Bernardi, M. I. Alonso, A. R. Goñi, J. O. Ossó, and M. Garriga, Appl. Phys. Lett. **89**, 101921 (2006).
[8] A. Bernardi, J. O. Ossó, M. I. Alonso, A. R. Goñi, and M. Garriga, Nanotechnology **17**, 2602 (2006).
[9] J. Stangl, V. Holý, and G. Bauer, Rev. Mod. Phys. **76**, 725 (2004).
[10] Q. Xie, A. Madhukar, P. Chen, and N. P. Kobayashi, Phys. Rev. Lett. **75**, 2542 (1995).
[11] G. S. Solomon, J. A. Trezza, A. F. Marshall, and J. S. Harris, Phys. Rev. Lett. **76**, 952 (1996).
[12] C. Colvard, T. A. Gant, M. V. Klein, R. Merlin, R. Fischer, H. Morkoc, and A. C. Gossard, Phys. Rev. B **31**, 2080 (1985).
[13] D. J. Lockwood, M. W. C. Dharma-wardana, J. M. Baribeau, and D. C. Houghton, Phys. Rev. B **35**, 2243 (1987).
[14] B. Jusserand and M. Cardona, in *Light Scattering in Solids V*, edited by M. Cardona and G. Guntherodt (Springer, Heidelberg, 1989), p. 49.
[15] T. Ruf, V. I. Belitsky, J. Spitzer, V. F. Sapega, M. Cardona, and K. Ploog, Phys. Rev. Lett. **71**, 3035 (1993).
[16] T. Ruf, J. Spitzer, V. F. Sapega, V. I. Belitsky, M. Cardona, and K. Ploog, Phys. Rev. B **50**, 1792 (1994).
[17] V. I. Belitsky, T. Ruf, J. Spitzer, and M. Cardona, Phys. Rev. B **49**, 8263 (1994).
[18] P. X. Zhang, D. J. Lockwood, and J. M. Baribeau, Can. J. Phys. **70**, 843 (1992).

[19] A. Mlayah, R. Grac, G. Armelles, R. Carles, A. Zwick, and F. Briones, Phys. Rev. Lett. **78**, 4119 (1997).
[20] M. Trigo, A. Fainstein, B. Jusserand, and V. Thierry-Mieg, Phys. Rev. B **66**, 125311 (2002).
[21] P. Lacharmoise, A. Fainstein, B. Jusserand, and V. Thierry-Mieg, Appl. Phys. Lett. **84**, 3274 (2004).
[22] M. Giehler, T. Ruf, M. Cardona, and K. Ploog, Phys. Rev. B **55**, 7124 (1997).
[23] M. Cazayous, J. R. Huntzinger, J. Groenen, A. Mlayah, S. Christiansen, H. P. Strunk, O. G. Schmidt, and K. Eberl, Phys. Rev. B **62**, 7243 (2000).
[24] M. Cazayous, J. Groenen, J. R. Huntzinger, A. Mlayah, and O. G. Schmidt, Phys. Rev. B **64**, 033306 (2001).
[25] M. Cazayous, J. Groenen, A. Zwick, A. Mlayah, R. Carles, J. L. Bischoff, and D. Dentel, Phys. Rev. B **66**, 195320 (2002).
[26] M. Cazayous, J. Groenen, J. Brault, A. Gendry, U. Denker, and O. G. Schmidt, Physica E (Amsterdam) **17**, 533 (2003).
[27] M. Cazayous, J. Groenen, J. R. Huntzinger, A. Mlayah, U. Denker, and O. G. Schmidt, Mater. Sci. Eng., B **88**, 173 (2002).
[28] A. Bernardi, J. S. Reparaz, A. R. Goñi, M. I. Alonso, and M. Garriga, Phys. Status Solidi B **244**, 76 (2007).
[29] C. Colvard, R. Merlin, M. V. Klein, and A. C. Gossard, Phys. Rev. Lett. **45**, 298 (1980).
[30] B. Jusserand, F. Alexandre, J. Dubard, and D. Paquet, Phys. Rev. B **33**, 2897 (1986).
[31] P. V. Santos, L. Ley, J. Mebert, and O. Koblinger, Phys. Rev. B **36**, 4858 (1987).